Title: Characterisation and fundamental insight into the formation of new solid state, multicomponent systems of propranolol

Author: Klaudia Bialek, Żaneta Wojnarowska, Brendan Twamley, Lidia Tajber.

UNIWERSYTET ŚLĄSKI W KATOWICACH

Biblioteka Uniwersytetu Śląskiego

Ministerstwo Nauki i Szkolnictwa Wyższego

Characterisation and fundamental insight into the formation of new solid state, multicomponent systems of propranolol

Klaudia Bialek [a], Zaneta Wojnarowska [a,b], Brendan Twamley [c], Lidia Tajber [a,*]

[a] *School of Pharmacy and Pharmaceutical Sciences, Trinity College Dublin, College Green, Dublin 2, Ireland*
[b] *Institute of Physics, University of Silesia, SMCEBI, 75 Pulku Piechoty 1A, 41-500 Chorzow, Poland*
[c] *School of Chemistry, Trinity College Dublin, College Green, Dublin 2, Ireland*

ARTICLE INFO

ABSTRACT

The physiochemical properties of acidic or basic active pharmaceutical ingredients (APIs) can be optimised by forming salts with different counterions. The aim of this work was to synthesise a novel salt of propranolol (PRO) using sebacic acid (SEBA) as the counterion and to gain mechanistic understanding of not only the salt formation, but also its eutectic phase formation with SEBA. Thermal analysis showed a solid-state reaction occurring between PRO and SEBA leading to the formation of dipropranolol sebacate (DPS) melting at app. 170 °C and the eutectic composed of DPS and SEBA melting at app. 103 °C, comprising 0.33 mol fraction of PRO as determined by the Tammann plot. X-ray diffraction and Fourier-transform infrared spectroscopy (FTIR) confirmed the identity of the new multicomponent phases of PRO. DPS can be conveniently obtained by heat-induced crystallisation, grinding and conventional solvent crystallisation. Detailed analysis by FTIR revealed H-bond interactions between DPS and SEBA at the inter-phase in the eutectic. Bravais, Friedel, Donnay and Harker crystal morphology coupled with full interaction maps analysis allowed to understand further the nature of interactions which led to formation of the eutectic phase. This work contributes to furthering research on multicomponent pharmaceutical systems to harness their full potential.

1. Introduction

Adequate aqueous solubility of orally administrated active pharmaceutical ingredients (APIs) is essential to ensure good bioavailability (Savjani et al., 2012). Nevertheless, up to 90% of APIs in the development stage may be considered as poorly soluble (Ting et al., 2018) and thus are more likely to fail during late-stage drug development. Therefore, the solubility problem should be overcome as early as possible by developing more soluble forms of drugs. The search for new forms of APIs, which have desirable properties, has become of paramount importance to the pharmaceutical industry in recent years. Alternative forms of API may include, but are not limited to, polymorphs, salts, cocrystals, ionic liquids or eutectics. Since many drugs are either weak acids or weak bases, the salt formation is by far the easiest way to optimise chemical and physical properties of poorly soluble APIs. The salt formation strategy can not only increase API solubility (Serajuddin, 2007), but it can also be used to improve stability (Sigfridsson et al., 2018), permeability (Mannava et al., 2020) and well as efficacy and release profiles.

Solvent-free, green synthesis is drawing attention of the pharmaceutical industry. Mechanochemistry offers environmentally friendly synthesis since no solvent waste is produced and excess of reagents is not required. Furthermore, it allows the use of solvent and/or heat sensitive reactants and products (Mottillo and Friščić, 2017). In recent years there has been an increased amount of accounts published on the mechanochemical approach to salt and co-crystal formation (Évora et al., 2019). Solid state reactions have also been studied in the context of stability of pharmaceutical formulations (Feng and Li, 2005). Solvent-free crystallisation methods include contact formation, solid-state grinding/ball milling and heat-induced crystallisation (Karimi-Jafari et al., 2018). With ball milling being the well-established method for forming salts and co-crystals, hot-melt extrusion, as scalable method of heat-induced crystallisation, is becoming a popular technology in salt/co-crystal formation in the solid state (Bookwala et al., 2018). Examples of multicomponent systems synthesised by solvent-free methods include an indomethacin/tromethamine salt (Bookwala et al., 2018), lamotrigine salts and co-crystals with xanthines and pyridinecarboxamides (Évora et al., 2019) and crystalline and amorphous salts of ciprofloxacin

---

(Paluch et al., 2013).

Propranolol (PRO) is a first-generation nonselective β-blocker (Kawanishi et al., 1992). It has traditionally been used in the treatment of cardiovascular diseases such as hypertension, cardiac arrhythmias and angina pectoris (Andreasen and Andersson, 2018). More recently it was introduced as a first-line therapy drug for infantile haemangioma, a common benign vascular tumour affecting around 5% of the infantile population (Léauté-Labrèze et al., 2017; Wagner et al., 2018). PRO is a poorly soluble weak base (609.4 mg/L) (Ferrari et al., 2004), thus it is marketed as the hydrochloride salt (PRO·HCl), which has solubility of 97.9 g/L (Thomas and Rubino, 1996). The hydrochloride is the most frequently used counterion in the pharmaceutical salt formation. It is used in app. 40% of all pharmaceutical salts formed (Paulekuhn et al., 2007). Despite the significant improvement in the solubility, PRO is poorly bioavailable (13–23%). Also, it undergoes extensive hepatic first-pass metabolism (Al Shaker et al., 2017). Low bioavailability of PRO can lead to a patient receiving an inconsistent dose which impairs achieving a therapeutic effect and causes unwanted side effects (Pathak and Raghuvanshi, 2015). Over the years, many attempts have been made to improve the biopharmaceutical properties of PRO by forming salts with counterions other than the hydrochloride. Stepanovs and co-workers developed a series of salts, cocrystals and solvates of PRO with oxalic, maleic and fumaric acids (Stepanovs et al., 2015). The developed salts, due to lower solubility than the PRO·HCl form, were considered as promising candidates for extended-release formulations. Compared with immediate-release tablets, extended-release formulations could decrease fluctuations of drug concentration in serum reducing side effects. Topical administration of PRO has also been explored. It has been shown that a salt formed between PRO and capric acid is capable of permeation through human skin by an ion-pair mechanism (Stott et al., 2001).

The chemical structure of PRO, shown in Fig. 1, comprises a secondary amine group, which potentially can act as a hydrogen bond donor and/or acceptor. Since PRO is a weak base with a pK_a of 9.7, a possibility of salt and co-crystal formation with an acidic counterion should be investigated. In the current study, we have selected sebacic acid (SEBA) as a potential beneficial counterion. SEBA is a dicarboxylic acid with a carbon chain length of 10. Dicarboxylic acids are used as counterions since they are multi-ionisable and phases with different stoichiometries may be formed. The carboxylic groups on both ends of the acid can act as a hydrogen bond donor, while the amine of PRO can act as a hydrogen bond acceptor. The pK_a difference between PRO and SEBA is greater than 3 (pK_a PRO = 9.7, pK_a SEBA = 4.7, ΔpK_a = 5), therefore a salt formation is expected for this system (Childs et al., 2007). Furthermore, SEBA is a pharmaceutically acceptable acid. It has been used to synthesise a range of cocrystals with several APIs such as sildenafil (Sanphui et al., 2013), isoniazid (Sarcevica et al., 2013), pyrazinamide (Wang et al., 2015) and apatinib (Zhu et al., 2018). PRO has been found to have irritative and ulcerogenic effect on oesophagus, similar to another β-blocker, alprenolol (Olovson et al., 1983). It has been reported that the use of SEBA as counterion to form a salt of alprenolol reduced its ulcerogenic and irritative effect (Olovson et al.,

1986). Therefore, the use of SEBA as a counterion in a PRO salt may also reduce its ulcerogenic effect.

The key aim of this study was to develop novel multicomponent systems, possibly a salt, of PRO with SEBA. PRO has already shown the ability to form a salt and eutectic forms with capric acid, which is a monocarboxylic acid with a carbon chain length of 10 (Stott et al., 1998), thus SEBA is the corresponding dicarboxylic acid. Therefore, the work presented here investigates how the inclusion of another carboxylic group in capric acid may change the propensity of PRO to form binary systems. We have explored different solvent-free approaches to the salt formation. The new solid-state forms composed of PRO and SEBA were investigated by detailed thermal analysis studies and construction of phase diagrams, further supported by powder X-ray diffraction and infrared spectroscopy to elucidate the usefulness of using SEBA as the counterion in PRO binary phases. Finally, computational studies were performed to understand intermolecular interactions between the different forms of PRO leading to the eutectic phase formation between the new salt and SEBA.

2. Materials and methods

2.1. Materials

Propranolol hydrochloride (PRO·HCl) was obtained from Glentham Life Sciences (UK) as a racemic mixture. Sebacic acid (SEBA) was purchased from Sigma Aldrich Chemie GmbH (Germany) and was used as supplied. Both chemicals had a purity of at least 99%. Ethanol was obtained from Fisher Scientific (UK) and was of HPLC grade. All other chemicals and solvents were of analytical grade.

2.2. Methods

2.2.1. Synthesis of propranolol base

Propranolol base (PRO) was obtained from its hydrochloride form. A quantity of 2 g of PRO·HCl was dissolved in 100 mL of deionised water. A saturated aqueous $NaHCO_3$ solution was added to the PRO·HCl solution until pH of 9 was reached while constantly stirring using a magnetic stirrer (Stuart SD162 Hotplate stirrer, UK) at a speed of 1000 rpm. A white suspension of PRO was obtained under these conditions, which was then filtered under vacuum using a ceramic Buchner flask with a 0.45 μm polypropylene membrane disc filter. The wet precipitate was washed with 50 mL of deionised water to eliminate any remaining water-soluble residues and dried at 70 °C for 2 h in an oven (Memmert UL 40, Germany).

2.2.2. Synthesis of dipropranolol sebacate salt

To obtain the dipropranolol sebacate (DPS) salt, PRO and SEBA were dissolved in hot ethanol in 1:1 M ratio in a 100 mL beaker. The reaction solution was constantly stirred using a magnetic stirrer (Stuart SD162 Hotplate stirrer, UK) at a speed of 1000 rpm to ensure complete dissolution of the components. The solution was then quench cooled by placing the beaker in an ice bath and kept at 4 °C overnight to allow salt
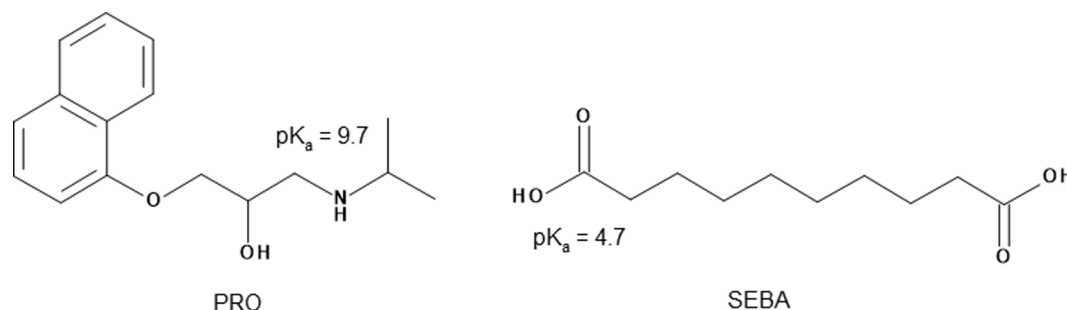

Fig. 1. Chemical structures and pK_a values of propranolol (PRO) and sebacic acid (SEBA).

precipitation. The precipitated salt was filtered under vacuum using a ceramic Buchner flask equipped with 0.45 µm polypropylene membrane disc filter. The salt was washed with 10 mL of ice-cold ethanol. DPS was dried overnight at 60 °C (Memmert UL 40, Germany) and its purity was confirmed by thermal analysis. The salt was stored in a 20 mL sealed amber glass jar at ambient temperature and moisture.

2.2.3. Preparation of PRO/SEBA and DPS/SEBA physical mixtures

Approximately 50 mg aliquots of physical mixtures of PRO/SEBA and DPS/SEBA were prepared by grinding accurately weighted quantities of the constituent powders, in appropriate molar ratios, using an agate mortar and pestle at room temperature. The molar fraction of PRO in the PRO/SEBA physical mixtures varied between 0 and 1. The quantity of drug in the DPS/SEBA mixtures is expressed as a molar fraction of PRO.

2.2.4. Preparation of samples for contact and grinding-assisted salt formation methods

PRO and SEBA were first pre-dried in the Memmert UL 40 oven at 70 °C for 1 h. For the contact salt formation method, pre-dried PRO and SEBA powders in the 2:1 M ratio were mixed gently in a 20 mL glass vial with a spatula. A total quantity of 20 mg mixture was prepared. For the grinding-assisted salt formation, 20 mg of the PRO/SEBA 2:1 M ratio mix were ground for 5 min in an agate mortar and pestle and then transferred to a 20 mL glass vial. All samples were hermetically sealed and stored at 25 and 60 °C in the oven (Memmert UL 40).

2.2.5. Preparation of the DPS and SEBA eutectic composition

20 mg of the eutectic was prepared by grinding SEBA (0.75 mmol) and DPS (0.25 mmol) for 5 min in an agate mortar and pestle. The sample was stored in a 20 mL sealed amber glass jar at ambient temperature and moisture.

2.2.6. Differential scanning calorimetry (DSC)

DSC measurements were carried out using a PerkinElmer Diamond DSC unit (USA). The unit was refrigerated using an ULSP B.V. 130 cooling system (Netherlands). Pyris software 9.01.0174 was used for data analysis. The DSC unit was calibrated using an indium standard. A heating rate of 10 °C/min was used (unless otherwise specified) with nitrogen (40 mL/min) as the purge gas. For the flash quenching step, a nominal cooling rate of 300 °C/min was applied. If required, the supercooled samples were re-heated at 10 °C/min. Approximately 5–10 mg samples were analysed in sealed 40 µL aluminium pans. The analysis was repeated at least in duplicate (Umerska et al., 2020).

2.2.7. Thermogravimetric analysis (TGA)

TGA was carried out using a Mettler Toledo TG50 TGA unit (Switzerland). The unit was coupled to a Mettler Toledo MT50 balance (Switzerland). Approximately 4 mg samples were analysed in non-sealed 40 µL aluminium pans. Samples were measured in triplicate by heating from 25 to 170 °C at a rate of 10 °C/min under nitrogen (40 mL/min) as a purge gas.

2.2.8. Powder X-ray diffraction (PXRD)

PXRD analysis was conducted using a Rigaku MiniFlexII Desktop X-ray diffractometer (Japan) with a Haskris cooling unit (USA). The tube (Cu, 1 kW normal focus) output voltage used was 30 kV and tube output current was 15 mA. Measurements were taken from 5 to 40˚on the 2theta scale at a step size of 0.05˚ per second at room temperature. PRO/SEBA samples were analysed "as is" or were heat pre-treated: samples containing 0.1–0.5 mol fraction of PRO were heated to 100 °C, cooled to room temperature and then analysed by PXRD; samples containing 0.6–0.9 mol fraction of PRO were heated to 120 °C, cooled to room temperature and then analysed.

2.2.9. Solid state Fourier transform infrared spectroscopy (FTIR)

FTIR was performed using a Spectrum One FT-IR spectrometer (PerkinElmer, Connecticut, USA) equipped with Universal ATR Sampling Accessory. The Spectrum Software version 6.1 was used. A spectral range of 450–4000 cm^{-1} and a resolution of 4 cm^{-1} were used. PRO/SEBA samples were analysed "as is" or were heat pre-treated: samples containing 0.1–0.5 mol fraction of PRO were heated to 100 °C, cooled to room temperature and then analysed by PXRD; samples containing 0.6–0.9 mol fraction of PRO were heated to 120 °C, cooled to room temperature and then analysed as described above in Section 2.2.8.

2.2.10. Single crystal X-ray diffraction (SCXRD)

Single crystals of the salt suitable for structural analysis were grown from an ethanolic solution of PRO and SEBA. The components in a 2:1 ratio (PRO:SEBA) were dissolved in 10 mL of HPLC grade ethanol in a glass vial. This solution was left under a fume hood at room temperature for solvent evaporation. Data for the sample were collected on a Bruker APEX DUO using Cu Kα radiation (λ = 1.54178 Å). The sample was mounted on a MiTeGen cryoloop and data collected at 100(2) K using an Oxford Cobra cryosystem. Bruker APEX3 software was used to collect and reduce data and determine the space group. Absorption corrections were applied using Bruker SADABS software. Structures were solved with the SHELXT structure solution program (Sheldrick, 2015a) using Intrinsic Phasing and refined with the SHELXL refinement package (Sheldrick, 2015b) using Least Squares minimisation. All non-hydrogen atoms were refined anisotropically. Hydrogen atoms were assigned to calculated positions using a riding model with appropriately fixed isotropic thermal parameters. Molecular graphics were generated using OLEX2 (Dolomanov et al., 2009). There is disorder in O15/O15a and C19/C20 both modelled in two positions with 88:12% occupancy. The disorder was modelled with restraints (SADI, SIMU, ISOR). Donor N-H hydrogen atoms located on the difference map and refined with restraints (DFIX). Crystallographic data for the structures in this paper have been deposited with the Cambridge Crystallographic Data Centre as supplementary publication no. 204963. Copies of the data can be obtained, free of charge, on application to CCDC, 12 Union Road, Cambridge CB2 1EZ, UK, (fax: +44-(0)1223-336033 or e-mail:deposit@ccdc.cam.ac.uk).

2.2.11. Crystal morphology of DPS

Crystals of DPS were obtained as described in Section 2.2.10. Micrographs of the crystal morphology were taken by a Q IMAGING Fast 1394 camera (Olympus, Japan) using an Olympus BX53 polarising optical microscope (Japan) equipped with a U-POT cross polarizer.

2.2.12. Computational analysis

Mercury 2020.3 software (UK) was used to calculate the PXRD powder patter of DPS based on the single-crystal X-ray structure and to predict the Bravais, Friedel, Donnay and Harker (BFDH) morphology of DPS and SEBA (CCDC code SEBAAC05 (Thalladi et al., 2000)). Mercury software was also used to generate full interactions map. The set of probes: uncharged NH, carbonyl oxygen and alcohol oxygen were used to provide an interaction map indicative of hydrogen bond acceptors (shown in red) and donors (shown in blue). Map contour levels and hotspots were applied to indicate how likely interactions are to occur. The higher the opacity of the contour, the higher the chances of interactions.

3. Results and discussion

3.1. Thermal analysis of binary physical mixtures of PRO and SEBA

DSC thermograms for the first heating cycle of PRO, SEBA and their physical mixtures are shown in Fig. 2a. Thermal analysis found that the melting temperature of pure PRO was 91.8 °C, which is in a good agreement with the literature value of 92.9 °C (Neau et al., 1993). All
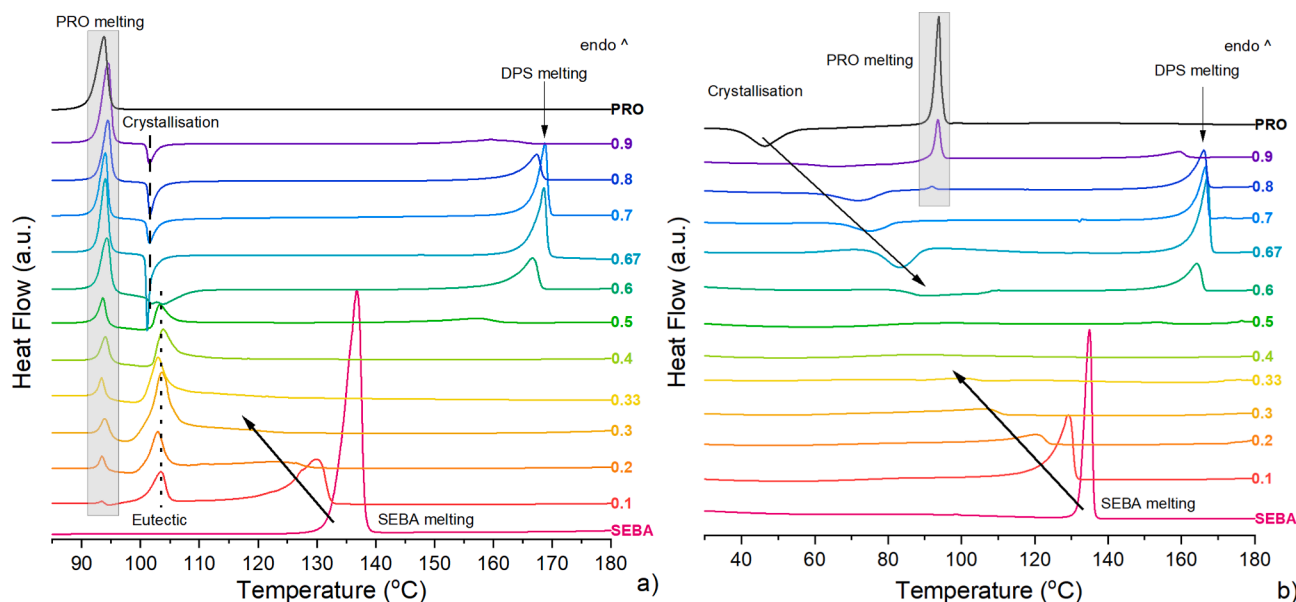
Fig. 2. Thermal analysis of binary physical mixtures of PRO and SEBA: a) DSC traces of PRO/SEBA physical mixtures from the first heating cycle, b) DSC traces of PRO/SEBA physical mixtures from the second heating cycle. The labels represent the mole fraction of PRO.

physical mixtures containing 0.67 and above mole fraction of PRO show similar thermal features. The first event can be attributed to the melting of PRO, which is then followed by an exothermic peak at around 100 °C and finally, a sharp endotherm is observed above 150 °C. The latter peak, with an onset at 166 °C, has the greatest enthalpy of melting (142.6 J/g) for the 2:1 mol/mole of PRO to SEBA. Considering that the melting point of SEBA is 133.5 °C, it can be hypothesised that the endotherm above 150 °C indicates melting of a new phase formed between PRO and SEBA. Yamashita et al. reported the appearance of an exothermic peak associated with cocrystal formation for 17 different cocrystals (Matsuoka et al., 2013). Based on the melting enthalpy values, it is possible that the stoichiometry of this new phase is 2 mol of PRO and 1 mol of SEBA (0.67 mol fraction of PRO). The thermogram of the mix containing 0.6 mol fraction of PRO is more complex and displays a "split" and broad exothermal event between 100 and 110 °C preceded by the PRO melting peak. Finally, an endotherm above 150 °C is present due to melting of the new phase. The DSC curves containing 0.5 mol of PRO and less showed, firstly, the melting endotherm of PRO at app. 92 °C followed by another endotherm appearing at a constant temperature of 103 °C. The second peak was followed by yet another endotherm in case of samples comprising 0.1–0.3 PRO, however the position of this peak was variable and seen to appear at a lower temperature with an increasing content of PRO. This peak can be ascribed to melting of SEBA. Considering that the position of the second endothermic peak, at around 103 °C, is relativity constant and unaffected by the sample composition, it might indicate the formation of a eutectic phase (Diarce et al., 2016), however it was unclear from the DSC data what the composition of this eutectic might be. Nevertheless, the greatest enthalpy of this peak was measured for the 1:2 mol/mole PRO to SEBA (0.33 mol fraction of PRO) sample, which was 172.3 J/g.

Following the first heating, the samples were quench cooled at a nominal cooling rate of 300 °C/min (Fig. S1) and subjected to the second heating cycle (at 10 °C/min). This approach was employed to examine the ability of samples to supercool and also to determine the magnitude of intermolecular forces in the disordered state (Koperwas et al., 2016; Umerska et al., 2020). SEBA and the samples containing 0.1–0.3 mol of PRO crystallised on cooling and, therefore, no glass transition temperatures (T_gs) were observed for these samples. The thermograms of these mixtures displayed an endotherm, most likely of the crystallised SEBA (Fig. 2b). All other samples showed T_gs (Fig. S2) and the compositional

relationship of the T_g values is presented in Fig. 3a. Interestingly, the mixture containing 0.67 mol of PRO had the highest T_g of 22 °C, which indicates that the intermolecular forces were the strongest at this composition (Umerska et al., 2020; Zotova et al., 2020). On the other hand, the sample comprising 0.33 PRO, which in the first heating showed the greatest enthalpy of the eutectic-like peak, had the lowest T_g, −25 °C, suggesting weakly interacting molecules (Wojnarowska et al., 2019; 2018). Crystallisation on the second heating cycle was detected for samples containing more than 0.5 mol fraction of PRO with the samples comprising 0.33–0.5 mol fraction of PRO showing excellent thermal stability on reheating (Fig. 2b). Again, the endothermal peak at around 166 °C for the 2:1 mol/mole PRO to SEBA was the one that was the most pronounced, therefore the crystallisation exotherm can be ascribed, at least in part, to crystallisation of this new phase. As compared to the first heating cycle the melting of PRO was only observed for samples at 0.9 and 0.8 mol fraction of PRO supporting the above suggestion that PRO is involved in formation of the new multicomponent phases.

As alluded to above, the DSC data suggested that the eutectic phase comprises around 0.33 mol of PRO as at this composition a single, sharp endotherm was produced, which also had the greatest enthalpy. However, one cannot simply determine the exact eutectic composition directly from DSC profiles, as eutectic phases do not always form in stoichiometric ratios (Cherukuvada and Nangia, 2014). The composition of a eutectic phase can accurately be confirmed by the construction of a Tammann plot (Fiandaca et al., 2020; Umerska et al., 2020). Thus, the enthalpy values of the eutectic endotherm assumed to be of a eutectic obtained from the first heating cycle were plotted against the mole fraction of PRO to obtain a triangular Tammann plot (Fig. 3b). Two lines are determined as best linear fits of the points and the eutectic composition is exactly at the intersection of these two lines giving the plot a triangular shape (Évora et al., 2016; Meltzer and Pincu, 2012). The eutectic composition, at 0.33 mol fraction of PRO, based on the Tammann plot agreed with that as determined directly from the DSC traces.

3.2. Identification of phases

Thermal analysis studies presented above suggested that two new, possibly multicomponent, phases might have formed during heating of PRO/SEBA physical mixtures, one which had a higher melting point
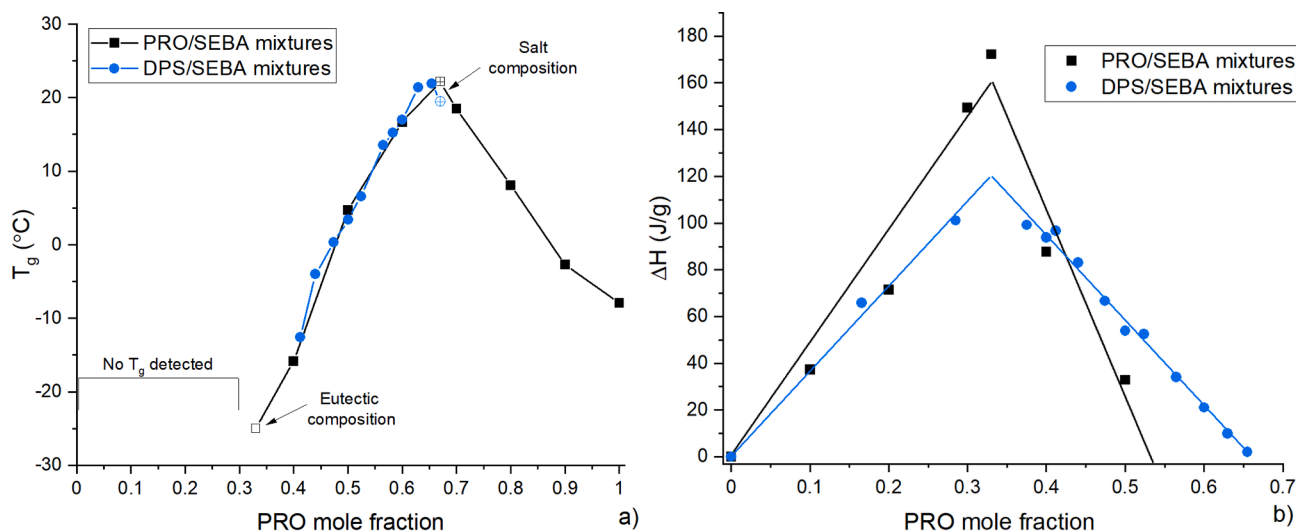
Fig. 3. a) Glass transition (T$_g$)-composition relationships for supercooled PRO/SEBA and DPS/SEBA mixtures. The lines are a guide for the eye. b) Tammann plots constructed using thermal data obtained from the first heating of physical mixtures (PRO/SEBA and DPS/SEBA). The lines are best fits to the data points.

than either PRO or SEBA and the other one was most likely to be a eutectic. Further analysis was performed to clarify the identity and composition of these phases.

The diffractograms of freshly prepared mechanical mixtures of PRO and SEBA showed peaks of the starting components (Fig. S3). However, the thermally treated samples (Fig. 4a) evidently show new peaks of a new phase. PXRD of the mixture at 0.67 mol fraction of PRO shows a distinctly different diffraction pattern with a characteristic peak at 6° 2θ in addition to other reflections in the diffractogram that cannot be assigned to any of the starting materials. The PXRD pattern of the heated mixture at 0.33 mol fraction of PRO, showed the presence of peaks that could be assigned to the new phase (6° and 16° 2θ) and SEBA (8°, 22° and 24° 2θ). The absence of peaks characteristic of PRO evidences that PRO does not seem to be directly involved in the formation of the eutectic. It can be concluded that the phase visible in the thermograms at around 103 °C is indeed a eutectic, but it is composed of SEBA and the new phase that melts at 166 °C.

FTIR analysis enabled further investigations into the nature of the interactions between PRO and SEBA. As highlighted in Introduction,

there is a possibility of ionic interactions occurring between these two components due to ionisable carboxylic groups present on SEBA and a basic secondary amine group, which may act as a proton acceptor, on PRO. The FTIR spectra of the heat-treated mixtures are shown in Fig. 4b. The spectrum of SEBA shows a characteristic absorption of the carbonyl group due to the presence of protonated carboxylic acid groups at 1687 cm^{-1} (Sailakshmi et al., 2012). The band is the broadest for pure acid due to the presence of strong intermolecular hydrogen bonding. Intensity of this peak decreases with an increase of PRO until it disappears completely when the PRO content increases to 0.7 mol fraction. At the same time, as the amount of PRO in the binary mixtures increases, new peaks at 1564 cm^{-1} and 1389 cm^{-1} appear corresponding to the asymmetric and symmetric vibrations of the carboxylate anion, respectively. These peaks have the highest intensity at 0.67 mol fraction of PRO. Therefore, it may be concluded that the 2:1 mol/mole PRO/SEBA composition (0.67 mol of PRO) forms a salt upon heating. The spectrum of system comprising 0.33 mol fraction PRO showed peaks characteristic of the salt and of SEBA, supporting the premise of a eutectic phase and discounting possibility of another salt.
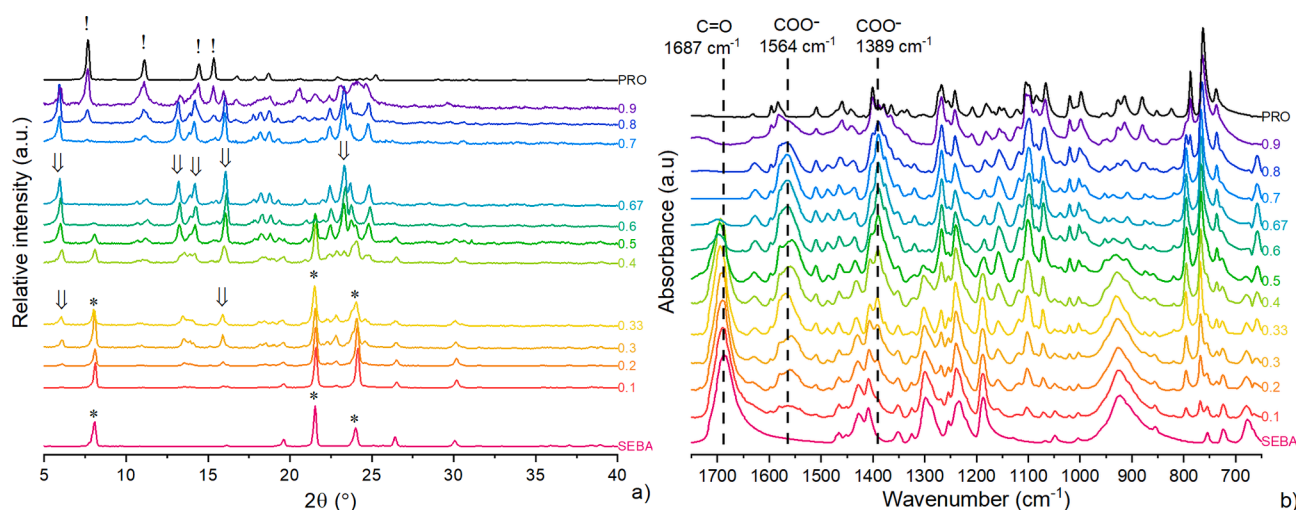

Fig. 4. a) PXRD patterns and b) FT-IR spectra of PRO and SEBA "as received" powders as well as PRO/SEBA physical mixtures subjected to thermal pre-treatment. The labels represent the mole fraction of PRO. The PRO/SEBA samples containing 0.1–0.5 mol fraction of PRO were heated to 100 °C, cooled to room temperature and then analysed. The PRO/SEBA samples containing 0.6–0.9 mol fraction of PRO were heated to 120 °C, cooled to room temperature and then analysed. The stars indicate characteristic peaks of SEBA, exclamation signs – PRO and arrows – DPS.

Based on the results of thermal analysis, PXRD and FTIR, a full phase diagram was constructed and the phases, as identified, are presented in Fig. 5. At higher contents of PRO, the melt of PRO facilitates the dissolution of SEBA and the phase, salt, crystallises as seen previously for e.g. ciprofloxacin succinate (Paluch et al., 2013). However, the eutectic phase, melting at around 100 °C and seen to form at lower PRO contents, appears to facilitate the solid-state reaction to the salt as the sharp exothermal event can no longer be observed, nevertheless the eutectic is composed of the salt and SEBA.

3.3. Crystallographic analysis of the salt

The salt was recrystallised from ethanol for the structure elucidation. To confirm its purity DSC analysis was performed. It was found that the onset of melting of pure salt is 169.5 °C and the enthalpy of this process is 178.2 J/g. TGA analysis of the salt revealed that it is thermally stable up to the melting point (170 °C) showing a weight loss of 1.3%. The weight loss up to 180 °C was 4.4%.

The structure of the new salt, dipropranolol sebacate (DPS), was determined by SCXRD and is shown in Fig. 6. The molecule crystallises in the centrosymmetric space group P$\bar{1}$, indicating the salt is racemic (Table S1). The asymmetric unit contains one molecule of the PRO cation and a half a molecule of SEBA, and the complete molecule is generated by symmetry in the ratio of 2:1 PRO/SEBA. There is disorder in the terminal isopropyl carbons (C19, C20) and in the hydroxyl O15/H14 positions (Fig. S4). In the major disordered moiety, each PRO cation is hydrogen bonded to the SEBA dianion via the protonated amine (asymmetric bifurcated N17…O21, 3.4084(16) Å; N17…O22, 2.7430 (16) Å) as well as the hydroxyl group (asymmetric bifurcated O15… O21, 2.6729(16) Å; O15…O22, 3.3171(18) Å). The minor disordered moiety displays a similar pattern, but with different hydrogen bond lengths from O15a…O21, 2.910(13) Å (Fig. S5). Further stabilisation by hydrogen bonding is seen via the amino N17 to a neighbouring SEBA oxygen N17…O21[iii], 2.7630(16) Å (symmetry generation iii = 2-x, 1-y, 1-z) and weaker CH…O interactions (C20…O22, 3.304(7) Å; C13… O22[ii], 3.2362(19) Å; symmetry generation ii = 1-x, 1-y, 1-z) also assist the structure stabilisation and connect the structure into a 3D network (Fig. S5). A calculated PXRD pattern, generated from the data above is shown in Fig. S6. The fit is visually reasonable and a Le Bail refinement yields Rp = 92.9% and Rwp = 90.1%. The predicted morphology based on the structure of DPS is also shown in Fig. 6b. It was found that the predicted morphology matches the predicted triclinic structure as shown in Fig. 6c.

3.4. Solvent-free formation of DPS

Since solvent-free approaches to the formation of multicomponent systems are preferred (Évora et al., 2019; Mottillo and Friščić, 2017; Zotova et al., 2020), upon establishing that the salt forms upon heating of the starting components (PRO and SEBA) to app. 105 °C (Fig. 2), an experiment was designed to investigate if it is possible for DPS to form without an excessive input of thermal energy. Two tests were carried out, one involving very gentle mixing (contact method) of PRO with SEBA in a 2:1 M ratio and the other was a grinding-assisted method. The samples were then stored at 25 and 60 °C and the reaction monitored by PXRD.

In relation to the contact method, there was no evidence of the salt formation after 14 days for the sample stored at 25 °C. Whereas a weak diffraction peak at 6° 2θ, unique to DPS, was observed after 14 days for the powder mixture stored at 60 °C (Fig. 7a). Considering the ground samples, the salt formation was seen after 7 days of storage at 25 and 60 °C (Fig. 7b). According to Paul and Curtin solid state reactions occur in four stages: 1) loosening of molecules at the reaction site; 2) molecular change; 3) solid solution formation and 4) separation of the product (Paul and Curtin, 1973). Step 1) is critical for the reaction to occur as it often requires an energy input. When the powders were just gently mixed with the spatula, the was no additional loosening of molecules from the surface and it is likely that crystal imperfections (defects) present on the "as supplied" samples were the only source of molecules available for the reaction. Molecular mobility was accelerated by applying the 60 °C thermal storage. The loosening of molecules at the reaction site can be greatly facilitated by grinding as mechanical forces are used (Takacs, 2014). As it is expected that the reaction rate is slow, no salt was observed immediately after grinding, however upon storage an appreciable level of conversion to the salt had occurred, enough for the PXRD to detect the new phase.

The formation of DPS at 25 and 60 °C is somewhat surprising, but it can be explained by the presence of crystal imperfections and/or disorder induced by grinding. For the fast conversion to the salt, melting of PRO (at around 90 °C) is still required, as shown in Fig. 2a, with the drug in the liquid state enabling dissolution of SEBA, the proton transfer between the species and then release of excess energy during the crystal formation, thus following the 4 stages of a solid state reaction described above. This can be simply carried out in an oven, however the possibility of a shear-induced disorder facilitating a further mobility of molecules at the contact sites, shown here on a small scale, may suggest that a fast conversion to the salt at larger scale can be achieved by e.g. hot melt extrusion, a technique combining the heat treatment coupled with the shear-induced disorder instigated by the moving screws (Lee et al., 2017). In relation to obtaining a crystalline product, the salt crystallisation process does not depend on the heating rate (Fig. S7), making the process easier to predict and control. Furthermore, as elucidated in Section 3.2, at low PRO contents, processing could be carried out in the eutectic melting zone, thus lowering the energy input even further.

3.5. DPS/SEBA interactions and physicochemical properties of the eutectic phase

Eutectics belong to a class of low-melting multicomponent crystalline solids (Cherukuvada and Nangia, 2014). The eutectic phase formation has been found as a useful strategy in improving solubility of APIs (Figueirêdo et al., 2017). It has been also successfully used to improve skin permeation of several APIs such as lidocaine/ prilocaine (Friedman et al., 2001) and ibuprofen (Stott et al., 1998). A eutectic may form if there are cohesive and non-covalent interactions between dissimilar components (Cherukuvada and Nangia, 2014). The existence and formation of a eutectic between compounds can be confirmed by
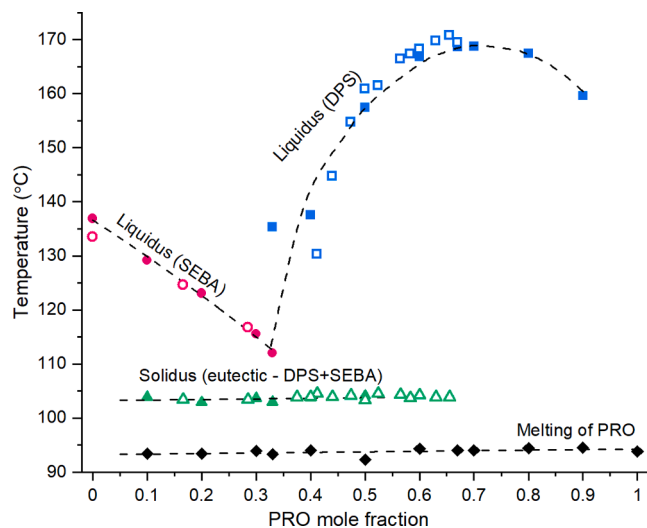

Fig. 5. Temperature/composition phase diagram for the PRO/SEBA system. Solid datapoints are based on first DSC heating of PRO/SEBA physical mixtures, while the open datapoints are based on first DSC heating of DPS/SEBA physical mixtures. The broken lines are a guide for the eye.
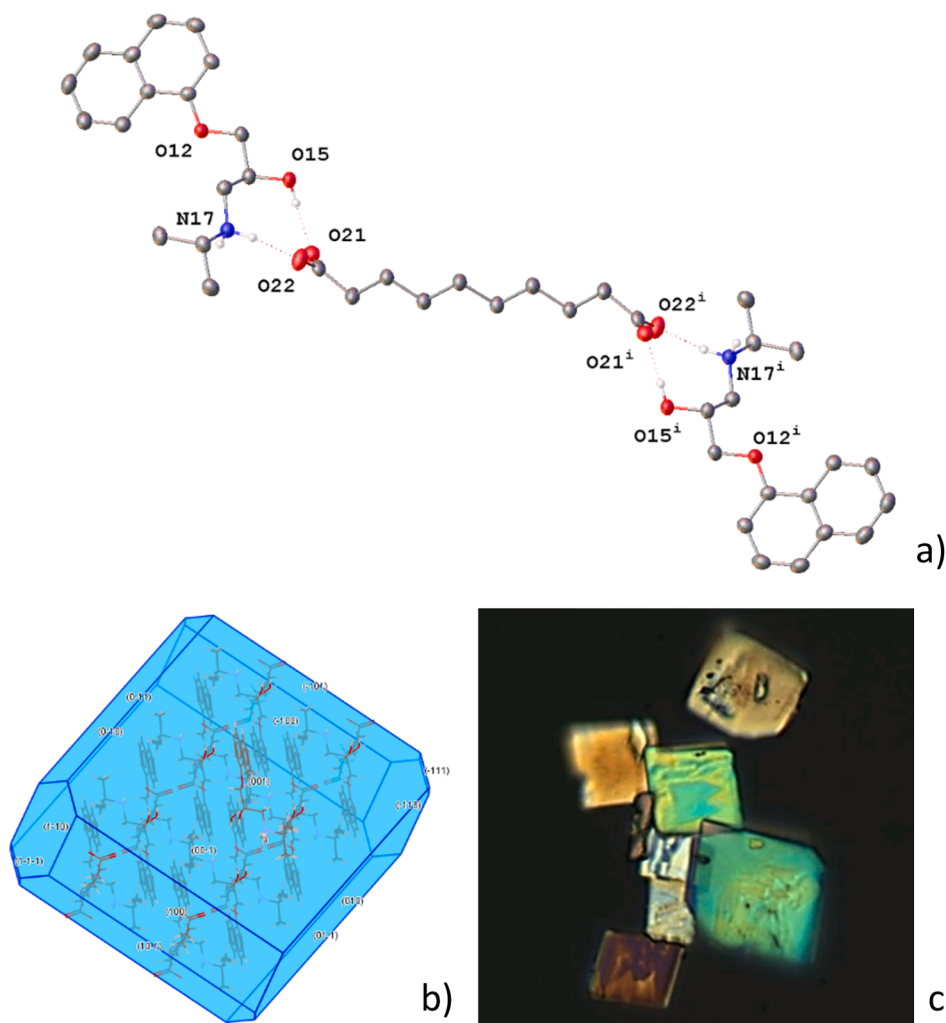
Fig. 6. a) Symmetry generated structure of DPS (symmetry transformation used to generate equivalent atoms i = 1-x, 1-y, -z) with atomic displacement shown at 50% probability and only hydrogen atoms involved in hydrogen bonding shown for clarity. Dotted lines indicate hydrogen bonding. Only the majority occupied (88%) disordered moiety is shown. b) Bravais, Friedel, Donnay and Harker (BFDH) predicted crystal morphology based on the SCXRD structure of DPS. c) Experimental morphology of DPS crystals.
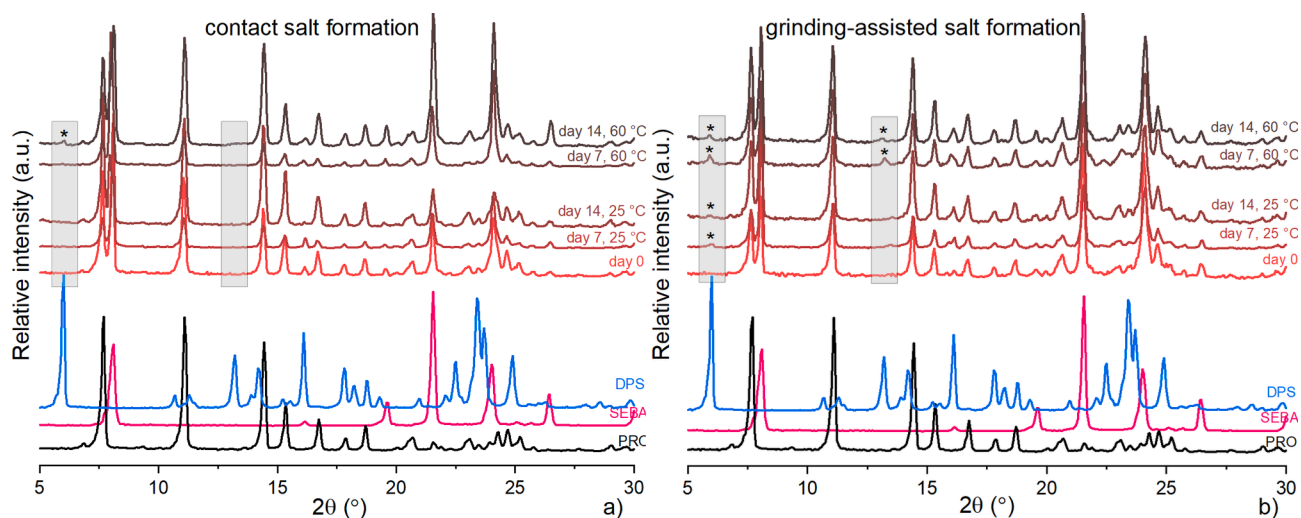

Fig. 7. a) PXRD of PRO/SEBA (2:1) samples prepared by prepared by gentle mixing with a spatula (contact method) and stored at 25 and 60 °C; b) PXRD of PRO/SEBA (2:1) samples prepared by prepared by grinding in a mortar and pestle (grinding-assisted method) and stored at 25 and 60 °C. Stars indicate the characteristic peaks of DPS.

constructing a phase diagram. There are two types of commonly recognised binary phase diagrams, which represent the eutectic formation. They may be either V- or W-shaped (Cherukuvada, 2016). The first involves formation of a eutectic between an acid and a base only, whereas the latter involves formation of a cocrystal (a new phase). The new phase then forms a eutectic either with a pure acid and/or a base.

There are only a few phase diagrams reported, which involve the salt formation and then that salt forming a eutectic (Cooke et al., 2010; Stott et al., 2001). Therefore, it appears that the DPS forming a eutectic system with SEBA belongs to this uncommon group of multicomponent pharmaceutical systems. The association of the salt into the eutectic allows to decrease of the melting point by nearly 70 °C, which may be advantageous for downstream processing.

Detailed thermal analysis of DPS/SEBA physical mixtures was conducted to understand the differences in behaviour between the components, especially the eutectic, when the *in situ* salt formation was eliminated. DSC thermograms (Figs. S8 and S9) confirmed that PRO does not directly partake in the formation of eutectic. As stated in Section 3.1, the eutectic composition determined from the Tammann plot based on the PRO/SEBA physical mixtures comprises 0.33 mol fraction of PRO, consistent with the data obtained using the DPS/SEBA systems (Fig. 3b). However, the enthalpies of the eutectic phase, as determined form the Tammann plots, were different, 161 J/g versus 120 J/g for the PRO/SEBA and DPS/SEBA mixtures, respectively. It may be explained by a better solubility or miscibility of components (DPS and SEBA) when the source of PRO was the salt itself, with no energy utilised for the *in situ* salt formation. The enthalpy difference can also be attributed to the presence of weak intermolecular forces between the components leading to cluster formation (Rastogi et al., 1981; Umerska et al., 2020). The T_g versus composition plot for the supercooled DPS/SEBA mixtures (Fig. 3a) showed that the samples containing below 0.4 mol fraction of PRO crystallised on cooling, therefore, no T_g was observed for these samples. However, unlike for the supercooled PRO/SEBA physical mixtures, no T_g was observed for the sample comprising 0.33 mol fraction of PRO which represents the eutectic. The overall trend of T_g versus PRO content was very similar with the T_g values decreasing as the composition of the eutectic was approached.

To elucidate the nature of interactions between the phases forming the eutectic, DPS and SEBA, a detailed infrared analysis was performed (Fig. 8a). Pronounced differences can be noticed associated with the SEBA vibrational groups (Max and Chapados, 2004; Sailakshmi et al., 2012). The broad band at 1687 cm^{-1} of pure SEBA, indicative of some dimer presence, is slightly shifted to higher wavenumbers in the eutectic (1694 cm^{-1}), this band is also narrower in comparison to that of pure SEBA. This strongly suggests H-bond rearrangement in the acid and a possibility of interaction with the salt. Notable changes are seen in the bands associated with the —OH moiety, demonstrated as shifts and narrowing of bending vibrations, in plane and out of plane (around 1410–1430 cm^{-1} and 920 cm^{-1}, respectively) of SEBA in the eutectic, suggestive of H-bond type interactions between the acid and DPS at the inter-phase, already suggested by the thermal analysis. Fig. 8b show the multicomponent microstructure of the eutectic made of multiple domains facilitating intimate contact between DPS and SEBA.

Since the eutectic microstructure is composed of domains of solid solutions held together by weak inter-phase boundaries (Fig. 8b) and the lattice structures of parent components remain principally unaffected (Cherukuvada and Nangia, 2014), a simulation was conducted using the BFDH representation of DPS and SEBA crystal morphologies and the full interaction map option to visualise the interaction sites (Mugheirbi and Tajber, 2015; Wood et al., 2013). The interaction map shows a possible interaction with hydrogen bond acceptors as red hot spots and possible interactions with hydrogen bond donors as blue hot spots. The higher the opacity of the contour, the greater the chance of the investigated interaction to take place (Wood et al., 2013). Inspecting the interaction map of a single SEBA molecule, it can be concluded that it can act as a H-bond donor and/or acceptor (Fig. 9a). The salt, due to the presence of several chemical groups can also interact with both H-bond acceptors and H-bond donors (Fig. 9b). BFDH predictions enable the surface area of key crystallographic faces to be determined. This information coupled with the interaction maps created for the BFDH crystal morphologies show that the principal interacting faces in the eutectic might be (1 0 0)
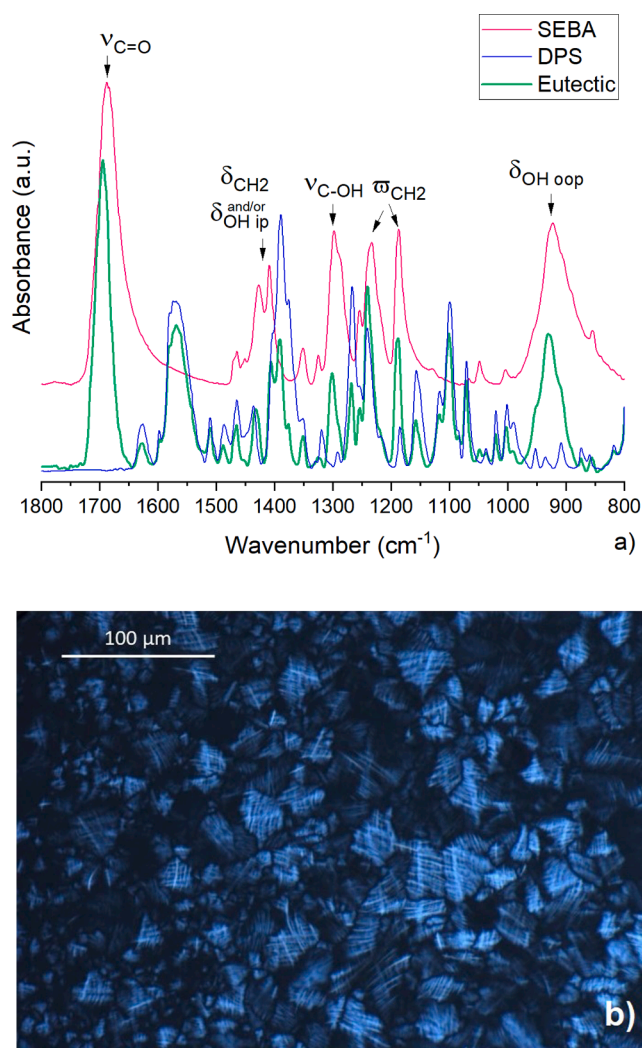

Fig. 8. a) FTIR spectra of SEBA, DPS and the eutectic phase. ν – stretching vibration, δ – bending vibration, ω – wagging vibration, ip – in plane, oop – out of plane. b) Polarised light microscopy of the eutectic at 25 °C.

and ($\bar{1}$0 0) of SEBA (52% surface area) as well as (0 0 1) and (0 0 $\bar{1}$) of DPS (45% surface area) (Fig. 9 c and d) as the interacting parts of the compounds will be exposed at those faces. Assuming hypothetically that in the eutectic the only interacting surfaces will be those primary faces, the theoretical composition of such a eutectic would be 0.63 mol fraction of SEBA and 0.37 mol fraction of PRO, which is very close to the experimental value of 0.33 mol fraction of PRO. Concluding, crystallographic analysis, like this presented here, can be helpful in understanding interactions at the inter-phase between components of a eutectic. To the best of our knowledge, BFDH/full interaction maps analysis has never been used for such a purpose.

4. Conclusions

This research was undertaken to comprehensively demonstrate the nature of interactions occurring between PRO and SEBA in the various solid-state phases. A binary phase diagram was successfully applied to prove the existence of two new forms of PRO: a salt (at 0.67 mol of PRO, dipropranolol sebacate) and a eutectic form (at 0.33 mol of PRO). It was shown that there is a possibility of *in situ* salt formation while thermally treating a physical mixture of PRO and SEBA, confirming that the heat-induced and solvent-free crystallisation of the salt is a viable route of manufacturing. Investigations into the mechanisms of the salt formation
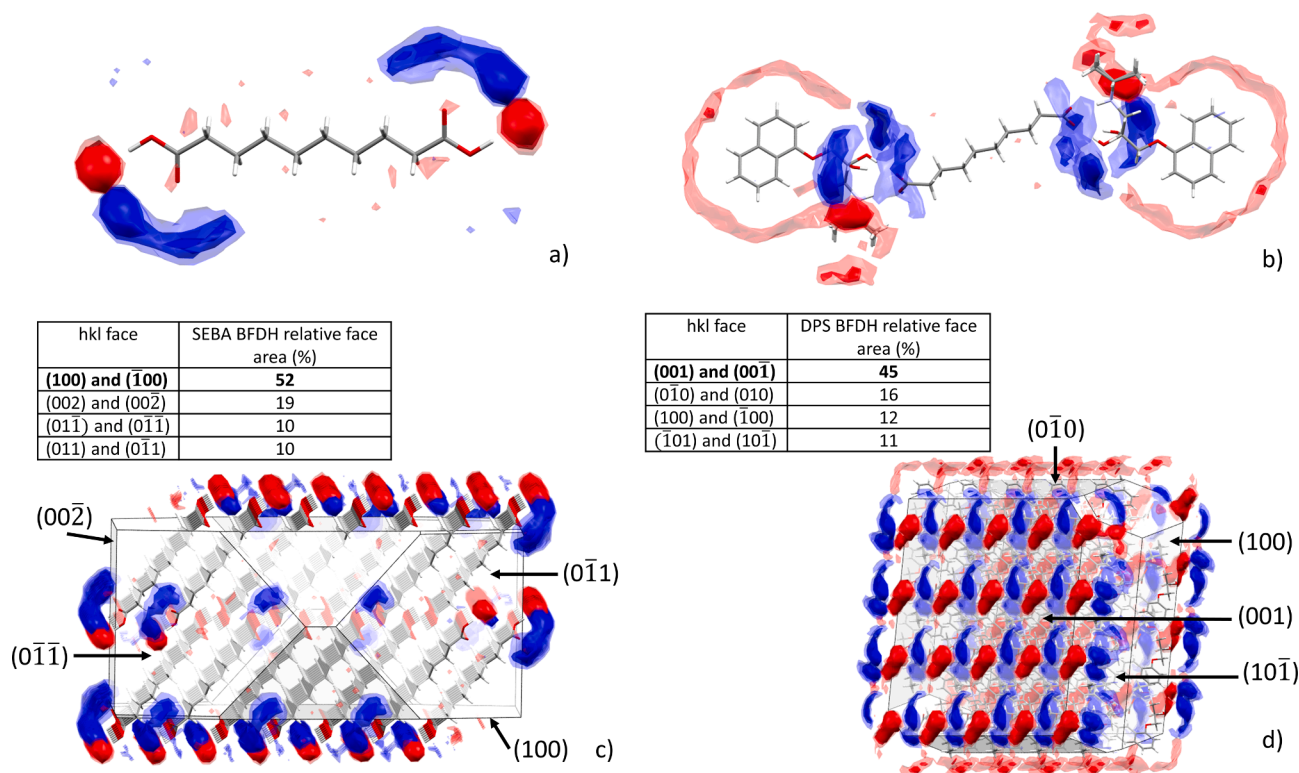
hkl face	SEBA BFDH relative face area (%)
(100) and (1̄00)	**52**
(002) and (002̄)	19
(011̄) and (011̄)	10
(011) and (011̄)	10

hkl face	DPS BFDH relative face area (%)
(001) and (001̄)	**45**
(01̄0) and (010)	16
(100) and (1̄00)	12
(1̄01) and (101̄)	11

Fig. 9. a) Full interaction map of SEBA (isolated molecule); b) Full interaction map of DPS (isolated molecule); c) Surface area of principal faces and full interaction map displayed on the BFDH morphology of SEBA and d) Surface area of principal faces and full interaction map displayed on the BFDH morphology of DPS. Full interaction maps illustrate possible hydrogen-bond donor and acceptor sites. H-bond acceptor sites were surveyed using carbonyl oxygen probes (red) and H-bond donor sites were surveyed using hydroxyl probes (blue).

showed that dipropranolol sebacate (DPS) can be obtained by mechanochemical means such as grinding as well as by crystallisation from solution. The crystal structure of the salt was solved, ultimately confirming ionisation between PRO and SEBA and the salt stoichiometry. DPS was found to interact *via* H-bond type interactions with SEBA to form a eutectic phase. The enthalpy of melting of the eutectic was used to generate a Tammann plot, which gave the exact composition of this phase (0.33 mol of PRO). Experimental analysis (infrared spectroscopy) and simulated data (BFDH crystal morphology coupled with full interaction maps) allowed to further understand the nature of interactions which led to the formation of the eutectic phase.

CRediT authorship contribution statement

Klaudia Bialek: Conceptualization, Methodology, Formal analysis, Investigation, Writing - original draft, Visualization. **Zaneta Wojnarowska:** Conceptualization, Methodology, Formal analysis, Investigation, Visualization. **Brendan Twamley:** Methodology, Formal analysis, Investigation, Resources, Writing - original draft, Visualization. **Lidia Tajber:** Conceptualization, Methodology, Formal analysis, Investigation, Resources, Writing - review & editing, Visualization, Supervision, Project administration, Funding acquisition.

Declaration of Competing Interest

The authors declare that they have no known competing financial interests or personal relationships that could have appeared to influence the work reported in this paper.

Acknowledgments

Appendix A. Supplementary material

Supplementary data to this article can be found online at https://doi.org/10.1016/j.ijpharm.2021.120605.

References

Al Shaker, H.A., Qinna, N.A., Badr, M., Al Omari, M.M.H., Idkaidek, N., Matalka, K.Z., Badwan, A.A., 2017. Glucosamine modulates propranolol pharmacokinetics via intestinal permeability in rats. Eur. J. Pharm. Sci. 105, 137–143. https://doi.org/10.1016/j.ejps.2017.05.012.

Andreasen, C., Andersson, C., 2018. Current use of beta-blockers in patients with coronary artery disease. Trends Cardiovasc. Med. 28, 382–389. https://doi.org/10.1016/j.tcm.2017.12.014.

Bookwala, M., Thipsay, P., Ross, S., Zhang, F., Bandari, S., Repka, M.A., 2018. Preparation of a crystalline salt of indomethacin and tromethamine by hot melt extrusion technology. Eur. J. Pharm. Biopharm. 131, 109–119. https://doi.org/10.1016/j.ejpb.2018.08.001.

Cherukuvada, S., 2016. On the issues of resolving a low melting combination as a definite eutectic or an elusive cocrystal: A critical evaluation. J. Chem. Sci. 128, 487–499. https://doi.org/10.1007/s12039-016-1055-7.

Cherukuvada, S., Nangia, A., 2014. Eutectics as improved pharmaceutical materials: Design, properties and characterization. Chem. Commun. 50, 906–923. https://doi.org/10.1039/c3cc47521b.

Childs, S.L., Stahly, G.P., Park, A., 2007. The salt-cocrystal continuum: The influence of crystal structure on ionization state. Mol. Pharm. 4, 323–338. https://doi.org/10.1021/mp0601345.

Cooke, C.L., Davey, R.J., Black, S., Muryn, C., Pritchard, R.G., 2010. Binary and ternary phase diagrams as routes to salt discovery: Ephedrine and pimelic acid. Cryst. Growth Des. 10, 5270–5278. https://doi.org/10.1021/cg1011296.

Diarce, G., Quant, L., Campos-Celador, Sala, J.M., García-Romero, A., 2016. Determination of the phase diagram and main thermophysical properties of the erythritol–urea eutectic mixture for its use as a phase change material. Sol. Energy Mater. Sol. Cells 157, 894–906. https://doi.org/10.1016/j.solmat.2016.08.016.

Dolomanov, O.V., Bourhis, L.J., Gildea, R.J., Howard, J.A.K., Puschmann, H., 2009. OLEX2: A complete structure solution, refinement and analysis program. J. Appl. Crystallogr. 42, 339–341. https://doi.org/10.1107/S0021889808042726.

Évora, A.O.L., Castro, R.A.E., Maria, T.M.R., Ramos Silva, M., Canotilho, J., Eusébio, M.E.S., 2019. Lamotrigine: Design and synthesis of new multicomponent solid forms. Eur. J. Pharm. Sci. 129, 148–162. https://doi.org/10.1016/j.ejps.2019.01.007.

Évora, A.O.L., Castro, R.A.E., Maria, T.M.R., Silva, M.R., Ter Horst, J.H., Canotilho, J., Eusébio, M.E.S., 2016. Co-crystals of diflunisal and isomeric pyridinecarboxamides-a thermodynamics and crystal engineering contribution. CrystEngComm 18, 4749–4759. https://doi.org/10.1039/c6ce00380j.

Feng, S., Li, T., 2005. Understanding solid-state reactions of organic crystals with density functional theory-based concepts. J. Phys. Chem. A 109, 7258–7263. https://doi.org/10.1021/jp0519666.

Ferrari, B., Mons, R., Vollat, B., Fraysse, B., Paxéus, N., Lo Giudice, R., Pollio, A., Garric, J., 2004. Environmental risk assessment of six human pharmaceuticals: Are the current environmental risk assessment procedures sufficient for the protection of the aquatic environment? Environ. Toxicol. Chem. 23, 1344–1354. https://doi.org/10.1897/03-246.

Fiandaca, M., Dalwadi, G., Wigent, R., Gupta, P., 2020. Ionic liquid formation with deep eutectic forces at an atypical ratio (2:1) of naproxen to lidocaine in the solid-state, thermal characterization and FTIR investigation. Int. J. Pharm. 575, 118946 https://doi.org/10.1016/j.ijpharm.2019.118946.

Figueirêdo, C.B.M., Nadvorny, D., de Medeiros Vieira, A.C.Q., Soares Sobrinho, J.L., Rolim Neto, P.J., Lee, P.I., de La Roca Soares, M.F., 2017. Enhancement of dissolution rate through eutectic mixture and solid solution of posaconazole and benznidazole. Int. J. Pharm. 525, 32–42. https://doi.org/10.1016/j.ijpharm.2017.04.021.

Friedman, P.M., Mafong, E.A., Friedman, E.S., Geronemus, R.G., 2001. Topical anesthetics update: EMLA and beyond. Dermatologic Surg. 27, 1019–1026. https://doi.org/10.1046/j.1524-4725.2001.01855.x.

Karimi-Jafari, M., Padrela, L., Walker, G.M., Croker, D.M., 2018. Creating cocrystals: A review of pharmaceutical cocrystal preparation routes and applications. Cryst. Growth Des. 18, 6370–6387. https://doi.org/10.1021/acs.cgd.8b00933.

Kawanishi, D.T., Reid, C.L., Morrison, E.C., Rahimtoola, S.H., 1992. Response of angina and ischemia to long-term treatment in patients with chronic stable angina: A double-blind randomised individualized dosing trial of nifedipine, propranolol and their combination. J. Am. Coll. Cardiol. 19, 409–417. https://doi.org/10.1016/0735-1097(92)90499-D.

Koperwas, K., Adrjanowicz, K., Wojnarowska, Z., Jedrzejowska, A., Knapik, J., Paluch, M., 2016. Glass-forming tendency of molecular liquids and the strength of the intermolecular attractions. Sci. Rep. 6, 1–10. https://doi.org/10.1038/srep36934.

Léauté-Labrèze, C., Harper, J.I., Hoeger, P.H., 2017. Infantile haemangioma. Lancet 390, 85–94. https://doi.org/10.1016/S0140-6736(16)00645-0.

Lee, H.L., Vasoya, J.M., De Lima Cirqueira, M., Yeh, K.L., Lee, T., Serajuddin, A.T.M., 2017. Continuous preparation of 1:1 haloperidol-maleic acid salt by a novel solvent-free method using a twin screw melt extruder. Mol. Pharm. 14, 1278–1291. https://doi.org/10.1021/acs.molpharmaceut.7b00003.

Mannava, M.K.C., Dandela, R., Tothadi, S., Solomon, K.A., Nangia, A.K., 2020. Naftopidil Molecular Salts with Improved Dissolution and Permeation. Cryst. Growth Des. 20, 3064–3076. https://doi.org/10.1021/acs.cgd.9b01689.

Matsuoka, K., Hisamatsu, T., Aoyagi, S., Motohashi, Y., Ikezawa, T., Tatsuno, S., Mizuno, Y., Nishida, J., 2013. Detection of cocrystal formation based on binary phase diagrams using thermal analysis. Pharm. Res. 30, 70–80. https://doi.org/10.1007/s11095-012-0850-1.

Max, J.J., Chapados, C., 2004. Infrared spectroscopy of aqueous carboxylic acids: comparison between different acids and their salts. J. Phys. Chem. A 108, 3324–3337. https://doi.org/10.1021/jp036401t.

Meltzer, V., Pincu, E., 2012. Thermodynamic study of binary mixture of citric acid and tartaric acid. Cent. Eur. J. Chem. 10, 1584–1589. https://doi.org/10.2478/s11532-012-0076-4.

Mottillo, C., Friščić, T., 2017. Advances in solid-state transformations of coordination bonds: From the ball mill to the aging chamber. Molecules 22. https://doi.org/10.3390/molecules22010144.

Mugheirbi, N.A., Tajber, L., 2015. Crystal habits of itraconazole microcrystals: unusual isomorphic intergrowths induced via tuning recrystallization conditions. Mol. Pharm. 12, 3468–3478. https://doi.org/10.1021/acs.molpharmaceut.5b00480.

Neau, S.H., Shinwari, M.K., Hellmuth, E.W., 1993. Melting point phase diagrams of free base and hydrochloride salts of bevantolol, pindolol and propranolol. Int. J. Pharm. 99, 303–310. https://doi.org/10.1016/0378-5173(93)90373-N.

Olovson, S.-G., Björkman, J.-A., Ek, L., Havu, N., 1983. The ulcerogenic effect on the oesophagus of three β-adrenoceptor antagonists, investigated in a new porcine oesophagus test model. Acta Pharmacol. Toxicol. (Copenh) 53, 385–391. https://doi.org/10.1111/j.1600-0773.1983.tb03439.x.

Olovson, S.-G., Havu, N., Regårdh, C.-G., Sandberg, A., 1986. Oesophageal ulcerations and plasma levels of different alprenolol salts: potential implications for the clinic. Acta Pharmacol. Toxicol. (Copenh) 58, 55–60. https://doi.org/10.1111/j.1600-0773.1986.tb00070.x.

Paluch, K.J., McCabe, T., Müller-Bunz, H., Corrigan, O.I., Healy, A.M., Tajber, L., 2013. Formation and physicochemical properties of crystalline and amorphous salts with different stoichiometries formed between ciprofloxacin and succinic acid. Mol. Pharm. 10, 3640–3654. https://doi.org/10.1021/mp400127r.

Pathak, K., Raghuvanshi, S., 2015. Oral bioavailability: issues and solutions via nanoformulations. Clin. Pharmacokinet. 54, 325–357. https://doi.org/10.1007/s40262-015-0242-x.

Paul, I.C., Curtin, D.Y., 1973. Thermally induced organic reactions in the solid state. Acc. Chem. Res. 6, 217–225. https://doi.org/10.1021/ar50067a001.

Paulekuhn, G.S., Dressman, J.B., Saal, C., 2007. Trends in active pharmaceutical ingredient salt selection based on analysis of the orange book database. J. Med. Chem. 50, 6665–6672. https://doi.org/10.1021/jm701032y.

Rastogi, R.P., Singh, N.B., Dwivedi, K.D., 1981. Solidification behaviour of addition compounds and eutectics of pure components and addition compounds. Berichte der Bunsengesellschaft für Phys. Chemie 85, 85–91. https://doi.org/10.1002/bbpc.19810850117.

Sailakshmi, G., Mitra, T., Sinha, S., Chatterjee, S., Gnanamani, A., Mandal, A.B., 2012. Suberic acid acts as a dissolving agent as well as a crosslinker for natural polymers (carbohydrate and Protein): A detailed discussion on the chemistry behind the interaction. J. Macromol. Sci. Part A Pure Appl. Chem. 49, 619–629. https://doi.org/10.1080/10601325.2012.696994.

Sanphui, P., Tothadi, S., Ganguly, S., Desiraju, G.R., 2013. Salt and cocrystals of sildenafil with dicarboxylic acids: Solubility and pharmacokinetic advantage of the glutarate salt. Mol. Pharm. 10, 4687–4697. https://doi.org/10.1021/mp400516b.

Sarcevica, I., Orola, L., Veidis, M.V., Podjava, A., Belyakov, S., 2013. Crystal and molecular structure and stability of isoniazid cocrystals with selected carboxylic acids. Cryst. Growth Des. 13, 1082–1090. https://doi.org/10.1021/cg301356h.

Savjani, K.T., Gajjar, A.K., Savjani, J.K., 2012. Drug Solubility: Importance and Enhancement Techniques. ISRN Pharm. 2012, 1–10. https://doi.org/10.5402/2012/195727.

Serajuddin, A.T.M., 2007. Salt formation to improve drug solubility. Adv. Drug Deliv. Rev. 59, 603–616. https://doi.org/10.1016/j.addr.2007.05.010.

Sheldrick, G.M., 2015a. SHELXT - Integrated space-group and crystal-structure determination. Acta Crystallogr. Sect. A Found. Crystallogr. 71, 3–8. https://doi.org/10.1107/S2053273314026370.

Sheldrick, G.M., 2015b. Crystal structure refinement with SHELXL. Acta Crystallogr. Sect. C Struct. Chem. C71, 3–8. https://doi.org/10.1107/S2053229614024218.

Sigfridsson, K., Ahlqvist, M., Lindsjö, M., Paulsson, S., 2018. Salt formation improved the properties of a candidate drug during early formulation development. Eur. J. Pharm. Sci. 120, 162–171. https://doi.org/10.1016/j.ejps.2018.04.048.

Stepanovs, D., Jure, M., Yanichev, A., Belyakov, S., Mishnev, A., 2015. Molecular salts of propranolol with dicarboxylic acids: Diversity of stoichiometry, supramolecular structures and physicochemical properties. CrystEngComm 17, 9023–9028. https://doi.org/10.1039/c5ce01408e.

Stott, P.W., Williams, A.C., Barry, B.W., 2001. Mechanistic study into the enhanced transdermal permeation of a model β-blocker, propranolol, by fatty acids: A melting point depression effect. Int. J. Pharm. 219, 161–176. https://doi.org/10.1016/S0378-5173(01)00645-7.

Stott, P.W., Williams, A.C., Barry, B.W., 1998. Transdermal delivery from eutectic systems: Enhanced permeation of a model drug, ibuprofen. J. Control. Release 50, 297–308. https://doi.org/10.1016/S0168-3659(97)00153-3.

Takacs, L., 2014. What is unique about mechanochemical reactions? Proc. 8th Int. Conf. Mechanochemistry Mech. Alloy. INCOME 2014 126, 1040–1043. https://doi.org/10.12693/APhysPolA.126.1040.

Thalladi, V.R., Nu, M., Boese, R., 2000. The melting point alternation in R, ω-alkanedicarboxylic acids. J. Am. Chem. Soc. 122, 9227–9236. https://doi.org/10.1021/ja0011459.

Thomas, E., Rubino, J., 1996. Solubility, melting point and salting-out relationships in a group of secondary amine hydrochloride salts. Int. J. Pharm. 130, 179–185. https://doi.org/10.1016/0378-5173(95)04269-5.

Ting, J.M., Porter, W.W., Mecca, J.M., Bates, F.S., Reineke, T.M., 2018. Advances in polymer design for enhancing oral drug solubility and delivery. Bioconjug. Chem. 29, 939–952. https://doi.org/10.1021/acs.bioconjchem.7b00646.

Umerska, A., Bialek, K., Zotova, J., Skotnicki, M., Tajber, L., 2020. Anticrystal engineering of ketoprofen and ester local anesthetics: Ionic liquids or deep eutectic mixtures? Pharmaceutics 12, 368. https://doi.org/10.3390/pharmaceutics12040368.

Wagner, M.J., Cranmer, L.D., Loggers, E.T., Pollack, S.M., 2018. Propranolol for the treatment of vascular sarcomas. J. Exp. Pharmacol. 10, 51–58. https://doi.org/10.2147/JEP.S146211.

Wang, J.R., Ye, C., Zhu, B., Zhou, C., Mei, X., 2015. Pharmaceutical cocrystals of the anti-tuberculosis drug pyrazinamide with dicarboxylic and tricarboxylic acids. CrystEngComm 17, 747–752. https://doi.org/10.1039/c4ce02044h.

Wojnarowska, Z., Smolka, W., Zotova, J., Knapik-Kowalczuk, J., Sherif, A., Tajber, L., Paluch, M., 2018. The effect of electrostatic interactions on the formation of pharmaceutical eutectics. Phys. Chem. Chem. Phys. 20, 27361–27367. https://doi.org/10.1039/c8cp05905e.

Wojnarowska, Z., Zotowa, J., Knapik-Kowalczuk, J., Tajber, L., Paluch, M., 2019. Effect of electrostatic interactions on the relaxation dynamics of pharmaceutical eutectics. Eur. J. Pharm. Sci. 134 https://doi.org/10.1016/j.ejps.2019.04.014.

Wood, P.A., Olsson, T.S.G., Cole, J.C., Cottrell, S.J., Feeder, N., Galek, P.T.A., Groom, C.R., Pidcock, E., 2013. Evaluation of molecular crystal structures using Full Interaction Maps. CrystEngComm 15, 65–72. https://doi.org/10.1039/c2ce25849h.

Zhu, B., Wang, J.R., Zhang, Q., Li, M., Guo, C., Ren, G., Mei, X., 2018. Stable cocrystals and salts of the antineoplastic drug Apatinib with improved solubility in aqueous solution. Cryst. Growth Des. 18, 4701–4714. https://doi.org/10.1021/acs.cgd.8b00684.

Zotova, J., Wojnarowska, Z., Twamley, B., Paluch, M., Tajber, L., 2020. Green Synthesis of lidocaine ionic liquids and salts: mechanisms of formation and interactions in the crystalline and supercooled states. ACS Sustain. Chem. Eng. 49, 18266–18276. https://doi.org/10.1021/acssuschemeng.0c06811.